Preprints of the 21st IFAC World Congress (Virtual)
Berlin, Germany, July 12-17, 2020

Fractional Order BPNN for Estimating State of Charge of Lithium-ion Battery under Temperature Influence ⋆

Yanan Wang * **Xiaozhong Liao** * **Da Lin** * **Xin Yang** *
Yangquan Chen **

* *School of Automation, Beijing Institute of Technology, Beijing 100081 China (e-mail: wangyn_bit@126.com)*
** *School of Engineering, University of California, Merced, CA 95343 USA (e-mail: ychen53@ucmerced.edu)*

Abstract: State of charge (SOC) estimation for lithium-ion battery (LIB) is always a vital issue for battery management system (BMS) of LIBs. Due to the complex nonlinear characteristics of LIBs, data-driven model and estimation methods have been proposed. Among them, back propagation neural network (BPNN) is one of the widely used machine learning (ML) method. To enhance the performance of BPNN of LIBs, a fractional-order BPNN (FO BPNN) based on fractional-order gradient method is designed for SOC estimation of LIB in this paper. Moreover, temperature acting as key factor is also taken into consideration. Hence, the charging or discharging current, voltage, and temperature are applied as the inputs of the proposed FO BPNN, and SOC is obtained from the network. By Dynamic Stress Test (DST) experiments under five different temperatures of four 18650 LIBs, it proves that the proposed FO BPNN is able to estimate SOC of LIBs accurately in a data-driven way.

Keywords: Fractional-order gradient method, back propagation neural network, state of charge estimation, lithium-ion battery, dynamic stress test.

1. INTRODUCTION

Lithium-ion Batteries (LIBs) are always the vital research objects due to the increasing energy consumption in modern applications, especially electric vehicles (EVs), however, LIBs are fragile and ageing is always a concern. Hence, state of charge (SOC) was proposed as a useful performance index to illustrate current capacity information of LIBs, and kinds of estimation methods have been designed for SOC, such as the well-known ampere-hour (Ah) method, and the open circuit voltage (OCV) measurement (Chaoui and Gualous, 2016; Wei et al., 2017). On the one side, monitoring and management of LIBs are faced with adaptive or online estimation requirements for battery management system (BMS) in EVs, and machine learning (ML) technologies just satisfy the dynamic and robust requirements (Zahid et al., 2017). Hence, data-driven models and estimation methods are developed based on ML (Li et al., 2019b). As a main investigated aspect of ML, several types of neural networks (NNs) were applied to SOC estimation, like back propagation neural network (BPNN) with backtracking search algorithm (BSA) (Hannan et al., 2018), and load-classifying NN. A specific NN, extreme learning machine (ELM), is also widely used to determine not only SOC of LIBs (Densmore and Hanif, 2016; Chin and Gao, 2018), but also state of health (SOH) (Pan et al., 2018) and remaining usage life (RUL) (Yang et al., 2018). These ML algorithms for SOC estimation always considers several variables as inputs, like current, temperature, power loss, and battery thermal factor through measurement or infrared images (Zahid et al., 2018), and take SOC as the only output. However, it is obvious that the structure of these ML frameworks are not too flexible, which may not satisfy the requirements of an online estimator or adaptive parameter networks for LIBs. Hence, an enhanced NN for SOC estimation should be found.

On the other side, among all the SOC estimation research of LIBs, fractional calculus has been applied to present constant phase element (CPE) and Warburg element (Zhang et al., 2019; Nasser-Eddine et al., 2019), which can reflect the mid-frequency reactions and low-frequency diffusion dynamics, according to the electrochemical impedance spectrum (EIS) of LIB (Guha and Patra, 2018). Moreover, fractional-order (FO) estimators have been proposed, and one of main aspects are the series of fractional-order Kalman filters (FO-KFs), such as extended KF (EKF) (Mawonou et al., 2019), adaptive EKF (AEKF)(Zhu et al., 2018), and dual KF (Li et al., 2019a). Among these advanced fractional-order methods of SOC estimation, fractional-order NNs are still not employed for LIBs. Hence, this paper combines fractional calculus and NNs to build an improved and more flexible NN for SOC estimation.

Based on the above introduction, this paper provides a BPNN model improved by fractional-order gradient method for estimating SOC of LIBs. With fractional-order gradient method, the proposed BPNN can hold

⋆ This work is supported by Nature Science Foundation of China (NSFC) Grant No. 61873035.

higher accuracy and robustness against disturbance of measurement process, which is suitable for real-time SOC estimation. The rest of this paper is divided into four parts: basic knowledge including the introduction of BPNN and fractional-order gradient method in section 2; the proposed fractional-order BPNN for estimating SOC of LIBs in section 3; the experiment results are provided to verify the proposed fractional-order BPNN in section 4; finally, some conclusions made in section 5.

2. BASIC KNOWLEDGE

2.1 State of Charge

SOC illustrates the remaining amount of available charge $Q(t)$ in a LIB, and can be expressed as the remaining percentage of a reference capacity Q_{ref} as follows

$$SOC = \frac{Q(t)}{Q_{ref}} = \underbrace{\frac{Q(t_0)}{Q_{ref}}}_{SOC_0} + \underbrace{\frac{\int_{t_0}^{t} I(\tau)d\tau}{Q_{ref}}}_{\Delta SOC(t)} = SOC_0 + \Delta SOC(t). \quad (1)$$

where $Q(t_0)$ is the initial capacity, and $I(\tau)$ is the charging or discharging current. In practice, the relaxation period is too long thus cannot obtain SOC_0 when LIB works in dynamic applications. Hence, how to measure real-time SOC is a key point of a adaptive BMS to prevent overcharge or overdischarge.

2.2 Back Propagation Neural Network

NN algorithm generally consists of the applied model, the optimal principle, and the strategy. BPNN has the multi-layers structure as shown in Fig. 1, and the back propagation is the strategy based on the gradient method (Rumelhart et al., 1988). From Fig. 1, the network contains the input layer with m neurons, hidden layers $(h_1, h_2, ..., h_l)$ with $n_p(p = 1, 2, ..., l)$ neurons, and output layer with q neurons, separately. Suppose the trained data for this networks is $(\mathbf{x}_i, \mathbf{y}_i), i = 1, 2, ..., N$, where $\mathbf{x}_i = (x_{i1}, x_{i2}, ..., x_{im})^{\mathrm{T}}$ and $\mathbf{y}_i = (y_{i1}, y_{i2}, ..., y_{iq})^{\mathrm{T}}$ are the input and the corresponding ideal output. To simplify expression, vectors $\mathbf{x}_i$ and $\mathbf{y}_i$ are presented as x and y. Let W_p and b_p be the weights and bias matrix connected the $(p-1)th$ hidden layer with the pth hidden layer, and $g(\cdot)$ and $f(\cdot)$ be the activation functions for the hidden and output layer. Then the forward propagation process can be presented as

$$\begin{aligned} a_p(x) &= W_p h_{p-1}(x) + b_p, \\ h_p(x) &= g(a_p(x)), p = 1, 2, ..., l \end{aligned} \quad (2)$$

where $a_p(x) = (a_p(x)_1, a_p(x)_2, ..., a_p(x)_{n_p})^{\mathrm{T}}$ is the input, and $h_p(x) = (h_p(x)_1, h_p(x)_2, ..., h_p(x)_{n_p})^{\mathrm{T}}$ is the output of the pth hidden layer, separately. The optimal principle, also called loss function, is usually chosen as the conventional square error function

$$L(f(x), y) = \frac{1}{2}\sum_{i=1}^{N} (\mathbf{y}_i - f(\mathbf{x}_i))^2. \quad (3)$$

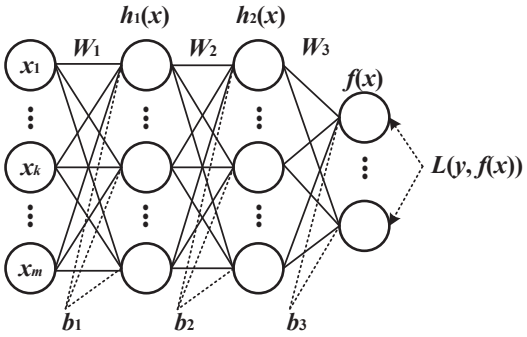

Fig. 1. Typical structure of BPNN with L hidden layers

For the back propagation of the neural network shown in Fig. 1, the gradient calculation starts from the output layer $f(x)$, and can be divided into the propagation of layer gradients, and the updates of weights matrix W_p and bias vectors b_p. The gradients of the pth hidden layer for the $kth, k = 1, 2, ..., N$ input sample are presented as

$$\begin{aligned} \frac{\partial L(f(x), y)}{\partial h_p^k(x)} &= W_{p+1}^k \frac{\partial L(f(x), y)}{\partial a_{p+1}^k(x)} \\ \frac{\partial L(f(x), y)}{\partial a_p^k(x)} &= \frac{\partial L(f(x), y)}{\partial h_p^k(x)} \cdot g'(a_p^k(x)) \\ &= W_{p+1}^k \frac{\partial L(f(x), y)}{\partial a_{p+1}^k(x)} \cdot g'(a_p^k(x)) \end{aligned} \quad (4)$$

where $\partial L(f(x), y)/\partial h_p^k(x)$ and $\partial L(f(x), y)/\partial a_p^k(x)$ are the gradients of the output $h_p^k(x)$ and the input $a_p^k(x)$ of the pth hidden layer, separately. Since the propagation starts from the output layer, we suppose that the gradients $\partial L(f(x), y)/\partial h_t^k(x)$ and $\partial L(f(x), y)/\partial a_t^k(x)$ of the tth, (t = p + 1, p + 2, ..., l, l + 1) layer are already known. Then the updates of the weights matrix and bias vectors are presented as

$$\begin{aligned} W_p^{k+1} &= W_p^k + \eta \cdot \frac{\partial L(f(x), y)}{\partial W_p^k} \\ b_p^{k+1} &= b_p^k + \eta \cdot \frac{\partial L(f(x), y)}{\partial b_p^k} \end{aligned} \quad (5)$$

where η is the learning rate of the weights matrix and bias vectors. Combined with (2), (5) can be presented as

$$\begin{aligned} W_p^{k+1} &= W_p^k + \eta \cdot \frac{\partial L(f(x), y)}{\partial a_p^k(x)} \cdot h_{p-1}^k(x) \\ b_p^{k+1} &= b_p^k + \eta \cdot \frac{\partial L(f(x), y)}{\partial a_p^k(x)} \end{aligned} \quad (6)$$

2.3 Fractional Order Gradient Method

Based on the BPNN introduced in section 2.2, the fractional-order gradient method can be obtained. The Caputo definition of the fractional-order derivative is employed in this paper as (Zhang et al., 2019)

$$ {}_{t_0}D_t^{\alpha} f(t) = \frac{1}{\Gamma(n-\alpha)} \int_{t_0}^{t} \frac{f^{(n)}(\tau)}{(t-\tau)^{\alpha-n+1}} \mathrm{d}\tau. \tag{7} $$

where ${}_{t_0}D_t^{\alpha}$ represents the Caputo type derivative operator, $n-1 < \alpha < n, n \in \mathbb{N}^+$, $\Gamma(\alpha) = \int_0^{\infty} x^{\alpha-1}\mathrm{e}^{-x}\mathrm{d}x$ is the Gamma function, t_0 is the initial time. (7) can be rewritten as the following form (Sheng et al., 2019)

$$ {}_{t_0}D_t^{\alpha} f(t) = \sum_{i=n}^{\infty} \frac{f^{(i)}(t_0)}{\Gamma(i+1-\alpha)} (t-t_0)^{i-\alpha}. \tag{8} $$

In this way, the corresponding fractional-order gradient method for the updates of weights matrix and bias vectors can be deduced from (5) as

$$ \begin{aligned} W_p^{k+1} &= W_p^k + \eta \cdot \frac{\partial^{\alpha} L(f(x),y)}{\partial (W_p^k)^{\alpha}} = W_p^k + \eta \cdot \frac{\partial L(f(x),y)}{\partial a_p^k(x)} \cdot \frac{\partial^{\alpha} a_p^k(x)}{\partial (W_p^k)^{\alpha}} \\ b_p^{k+1} &= b_p^k + \eta \cdot \frac{\partial^{\alpha} L(f(x),y)}{\partial (b_p^k)^{\alpha}} = b_p^k + \eta \cdot \frac{\partial L(f(x),y)}{\partial a_p^k(x)} \cdot \frac{\partial^{\alpha} a_p^k(x)}{\partial (b_p^k)^{\alpha}} \end{aligned} \tag{9} $$

From (9), the integer-order partial derivatives in (5) are replaced by the fractional-order partial derivatives. It is proved that the chain rule in (9) for fractional-order partial derivatives is valid when the loss function is the square error function in (3) (Sheng et al., 2019), while it needs to be noted that this chain rule is not always correct for all functions (Tarasov, 2016). In this way, the update equations of the propagation of layer gradients are still employed the integer-order ones in (4). Hence, the propagation between layers are remained integer-order ones, and the updates of weights matrix and bias are designed as fractional-order ones.

3. PROPOSED FRACTIONAL ORDER BPNN FOR LIBS

Based on the introduced fractional-order gradient method, a fractional-order BPNN is designed for estimating SOC of LIBs in this part. A simplified BPNN structure is chosen as only one hidden layer, so that the fractional-order BPNN includes an input layer, a hidden layer, and an output layer. The activation functions for the hidden layer and output layer are chosen as the log-sigmoid function

$$ S(net) = \frac{1}{1+\mathrm{e}^{(-net)}}. \tag{10} $$

where *net* means the inputs of the hidden layer or the output layer. The first order derivative of the log-sigmoid function is $S'(net) = S(net)(1-S(net))$. Hence, we can assume the input and output of the hidden layer are

$$ \begin{aligned} a_1^k(\mathbf{x_i}) &= W_1^k \mathbf{x_i} + b_1^k, \\ h_1^k(\mathbf{x_i}) &= S_1(a_1^k(\mathbf{x_i})) \end{aligned} \tag{11} $$

Similarly, the input and output of the output layer are

$$ \begin{aligned} a_2^k(\mathbf{x_i}) &= W_2^k h_1(\mathbf{x_i}) + b_2^k, \\ h_2^k(\mathbf{x_i}) &= f(\mathbf{x_i}) = S_2(a_2^k(\mathbf{x_i})) \end{aligned} \tag{12} $$

To make expression concise, $S_1(a_1(\mathbf{x_i}))$ and $S_2(a_2(\mathbf{x_i}))$ are presented as S_1 and S_2. According to Section 2.2 and 2.3, the updating equations with fractional-order gradients of weights matrix can be derived as

$$ \begin{aligned} W_2^{k+1} &= W_2^k + \eta \sum_{i=1}^{N} (\mathbf{y_i} - S_2)\delta_2 \cdot \frac{\partial^{\alpha} a_2^k(\mathbf{x_i})}{\partial (W_2^k)^{\alpha}} \\ W_1^{k+1} &= W_1^k + \eta \sum_{i=1}^{N} (\mathbf{y_i} - S_2)\delta_2 W_2^k \delta_1 \cdot \frac{\partial^{\alpha} a_1^k(\mathbf{x_i})}{\partial (W_1^k)^{\alpha}} \end{aligned} \tag{13} $$

where $\delta_2 = S_2(1-S_2), \delta_1 = S_1(1-S_1)$. Take $i=1$ in (8), then $\frac{\partial^{\alpha} a_p^k(\mathbf{x_i})}{\partial (W_p^k)^{\alpha}}, p = 1,2$ can be approximated as

$$ \begin{aligned} \frac{\partial^{\alpha} a_2^k(\mathbf{x_i})}{\partial (W_2^k)^{\alpha}} &= h_1^k(\mathbf{x_i}) \cdot \frac{1}{\Gamma(2-\alpha)} \left(W_2^k - W_2^0\right)^{1-\alpha} \\ \frac{\partial^{\alpha} a_1^k(\mathbf{x_i})}{\partial (W_1^k)^{\alpha}} &= \mathbf{x_i} \cdot \frac{1}{\Gamma(2-\alpha)} \left(W_1^k - W_1^0\right)^{1-\alpha} \end{aligned} \tag{14} $$

where W_2^0 and W_1^0 are the initial values of W_2^k and W_1^k. Take (14) into (13), we can obtain the discrete realization of the weights updating equations in FO BPNN as

$$ \begin{aligned} W_2^{k+1} &= W_2^k + \frac{\eta}{\Gamma(2-\alpha)} \sum_{i=1}^{N} (\mathbf{y_i} - S_2)\delta_2 \cdot h_1^k(\mathbf{x_i}) \left(W_2^k - W_2^0\right)^{1-\alpha} \\ W_1^{k+1} &= W_1^k + \frac{\eta}{\Gamma(2-\alpha)} \sum_{i=1}^{N} (\mathbf{y_i} - S_2)\delta_2 W_2^k \delta_1 \cdot \mathbf{x_i} \left(W_1^k - W_1^0\right)^{1-\alpha} \end{aligned} \tag{15} $$

The updating equations for the bias vectors are very similar to (15), so it would not be presented here. After designing the structure and iteration process of the FO BPNN, the inputs for LIBs need to be considered. Fig. 2 and Fig. 3 are the available capacity of four 18650 LIBs in five different temperatures, and the voltage and SOC curves of one 18650 LIB under dynamic stress test (DST), respectively. The rated capacity of the four 18650 LIBs is 2Ah, and the rated voltage is 3.7V. From Fig. 2 and Fig. 3, it is obvious that, not only the available capacity but also the real-time voltages and SOC values are varied in different temperatures. Hence, temperature needs to be considered in the FO BPNN for SOC estimation. Firstly, we have chosen three variables as the inputs of the FO BPNN, that is, the charging or discharging current, the voltage, and the temperature of LIB. Then, SOC is considered as the desirable output of the FO BPNN. Finally, the complete iteration process of the proposed FO BPNN for LIB can be concluded as the following steps:

(1) Step 1: Initialization of parameters of the FO BPNN, such as the initial values of weights matrix $W_p^0, p = 1,2$, bias vectors $b_p^0, p = 1,2$, learning rate η, and fractional order α.
(2) Step 2: Collecting the experimental data from DST as the current I, the voltage V, the temperature T, and the real SOC value. Then, the collected data is divided into training, validation, testing data.
(3) Step 3: Calculate the inputs $a_p^k(\mathbf{x_i}), p = 1,2$ and outputs $h_p^k(\mathbf{x_i}), p = 1,2$ of the hidden layer and the

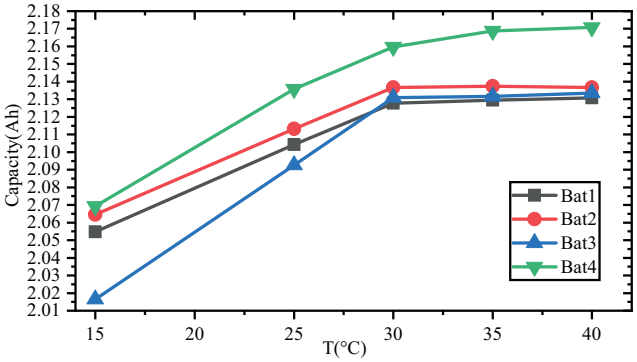

Fig. 2. The available capacity of four 18650 LIBs (rated capacity = 2Ah) in five temperatures, that is, 15°C, 25°C, 30°C, 35°C, and 40°C

output layer according to (11) and (12). Calculate the output square error $e^k = \frac{1}{2}\sum_{i=1}^{N}(\mathbf{y}_i - h_2^k(\mathbf{x_i}))^2$.

(4) Step 4: Back propagation from the output layer, and calculating the integer-order partial derivatives

$$\begin{aligned}
\frac{\partial L(f(x),y)}{\partial h_2^k(x)} &= \sum_{i=1}^{N}(\mathbf{y_i} - S_2),\\
\frac{\partial L(f(x),y)}{\partial a_2^k(x)} &= \sum_{i=1}^{N}(\mathbf{y_i} - S_2)\delta_2,\\
\frac{\partial L(f(x),y)}{\partial h_1^k(x)} &= \sum_{i=1}^{N}(\mathbf{y_i} - S_2)\delta_2 W_2^k,\\
\frac{\partial L(f(x),y)}{\partial a_1^k(x)} &= \sum_{i=1}^{N}(\mathbf{y_i} - S_2)\delta_2 W_2^k \delta_1.
\end{aligned} \tag{16}$$

Then, updating the weights matrix $W_p^0, p = 1, 2$ and bias vectors $b_p^0, p = 1, 2$ according to (13).

(5) Step 5: Validation check, and verify the output square error e^k. If passing the validation check and e^k satisfies the required value, go to Step 6; if not, go to Step 3.

(6) Step 6: Employing the testing data into the trained FO BPNN to analyze the effectiveness of the proposed FO BPNN.

It needs to be noted that the fractional order α of the fractional-order gradient method is currently set up as 0.9, while the influence of fractional order on the stability and performance of networks is another worthy investigated direction, we would conduct further research.

4. EXPERIMENT AND ANALYSIS

4.1 Experiment Setup

In this part, experiments are conducted to verify the proposed FO BPNN, results with analysis are provided in the following section. The four 18650 LIBs in Fig. 2 are considered as the tested objects and numbered as "Bat1, Bat2, Bat3, Bat4", and DST is conducted on the BTS-4 series battery tester produced by Shenzhen Neware Company to collect the data of current I, voltage V, and temperatures T. The employed 18650 LIB has 2Ah nominal capacity and 3.7V nominal voltage. All the four 18650 batteries were fully charged by constant-voltage

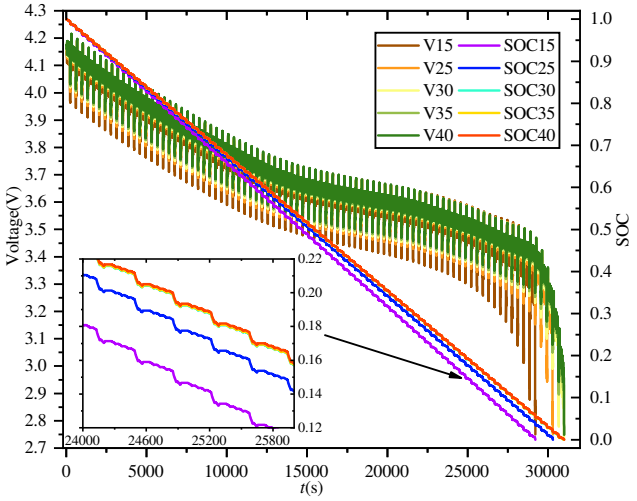

Fig. 3. The voltage and SOC curves of one 18650 LIB under DST in five temperatures, that is, 15°C, 25°C, 30°C, 35°C, and 40°C

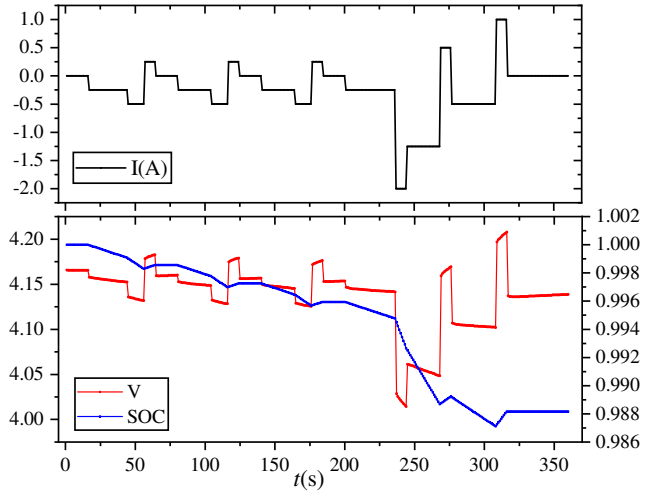

Fig. 4. The curves of current, voltage and SOC of Bat1 in a typical DST period under 25°C

constant-current method before DST. A typical DST lasts 360s, and the curves of charging or discharging current, voltage, and SOC are shown in Fig. 4. It needs to be noted that the real SOC values are calculated by ampere-hour integral method on the BTS-4 series battery tester.

Considering the influence of temperatures on SOC estimation, "Bat1-Bat4" are conducted the same DST process under 15°C, 25°C, 30°C, 35°C, and 40°C. Fig. 5 shows all the recorded temperatures curves of the four batteries "Bat1-Bat4". It can be observed that four batteries were tested under five temperatures, so that 20 groups of raw data were collected. From Fig. 3, same battery in the five different temperatures may present various behaviors, especially in 15°C and 25°C. As shown in Fig. 5, since the sampling time of BTS-4 series battery tester is 1s, the voltages of LIBs would not change so fast and every group of raw data is over 30000s. Hence, the 20 groups of raw data were smoothed by a low pass filter to avoid overfitting of the FO BPNN, then the final preprocessed data is reduced to about 6000s. After the preprocessing of the

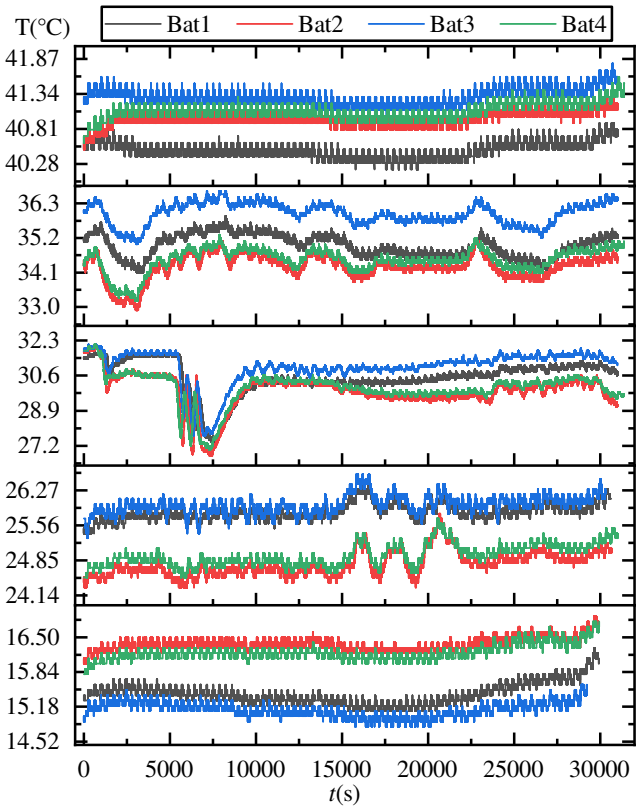

Fig. 5. The tempratures curves of the four batteries "Bat1, Bat2, Bat3, Bat4" during the DST process under 15°C, 25°C, 30°C, 35°C, and 40°C

20 groups of raw data, FO BPNN was trained based on these data and the steps in Section 3.

4.2 Results and Analysis

Figure 6 shows the voltage and SOC curves of the four 18650 batteries under 25°C, and it shows that the diversity of various batteries are relatively small but also taken into consideration. The FO BPNN is constructed in MATLAB, which has the same feedforward process with the integer-order BPNN, but the iteration equations of the weights matrix were revised according to (13). The training function was designed as fractional-order gradient methods with adaptive learning rate, to accelerate the convergence process and reduce the iteration epoch.

Fig. 7 and Fig. 8 are the results of the FO BPNN to estimate SOC of four 18650 LIBs. The hidden layer has 8 neurons, and the required performance error and the validation checks are set as 0.005 and 6. After the preprocessing by the filter, the input data including current I, voltage V, and temperature T have 89731 points, which are separated into 70% training data, 15% validation data, and 15% testing data. Fig. 7 is the performance error, which reached 0.0068819 at epoch 136 and was stopped by the mean square error check. The training result of the integer-order BPNN (IO BPNN) is also presented in Fig. 7 as a comparison to FO BPNN. It is obvious that the FO BPNN has faster training speed and smaller error than IO BPNN, which can only reach 0.00827.

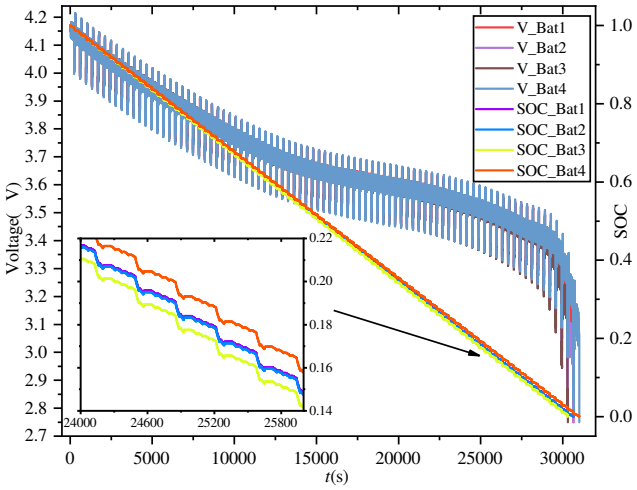

Fig. 6. The voltage and SOC curves of the four batteries "Bat1, Bat2, Bat3, Bat4" during the DST process under 25°C

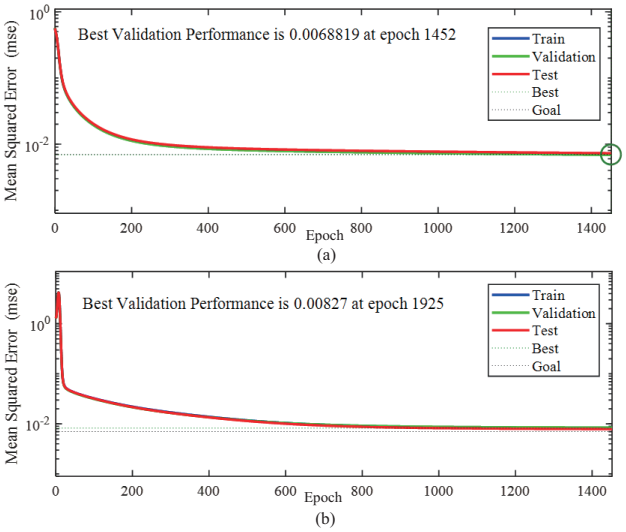

Fig. 7. The performance error curve of the proposed FO BPNN for SOC estimation of LIB, (a) FO BPNN, (b) IO BPNN

To further illustrate the performance of FO BPNN, the regression result is also provided in Fig. 8, which includes the regression results of the training, validation, and testing data, respectively. It can be obtained that the regression coefficient of the testing data can be $R = 0.98905$, which illustrates that the proposed FO BPNN can effectively estimate SOC for LIBs. Moreover, the regression coefficients of both FO BPNN and IO BPNN are listed in table 1. By comparison, the regression coefficients of FO BPNN are smaller than those of IO BPNN as shown in table 1. The regression coefficient of all data in FO BPNN can reach 0.98942, which is relatively higher than that of IO BPNN, which is 0.98796.

Table 1. The regression coefficients of both FO BPNN and IO BPNN

Type	Training	Validation	Testing	All
FO BPNN	0.98949	0.98947	0.98905	0.98942
IO BPNN	0.98802	0.98742	0.98821	0.98796

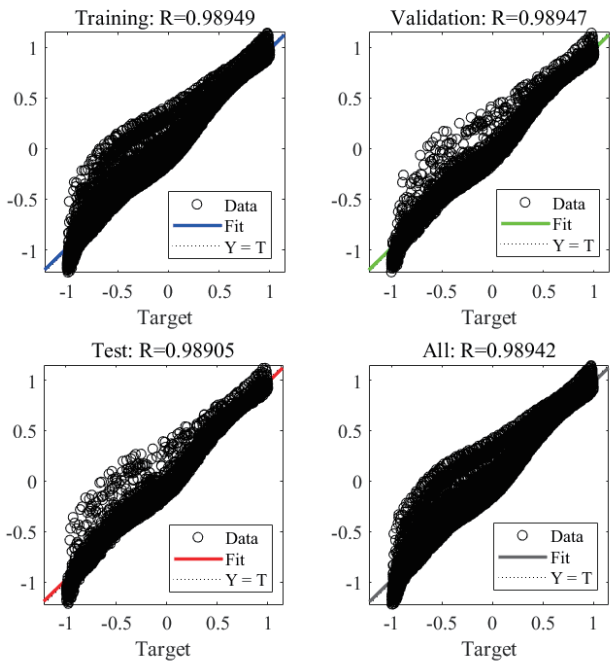

Fig. 8. The regression results of the proposed FO BPNN for SOC estimation of LIB

5. CONCLUSION

Based on the fractional-order gradient method, this paper presents a fractional-order BPNN for SOC estimation of LIBs. While the structure and the integer-order updates of layer gradients of integer-order BPNN remains, the updating equations of weights matrix and bias vectors are designed based on the fractional-order gradients. Since temperature acts as an important role in SOC estimation of LIBs, the proposed FO BPNN employs current, voltage, and temperature as the inputs of the network. A detail iterative process with six steps of the proposed FO BPNN is provided in Section 3. DST experiments under five different temperatures are conducted to verify the proposed FO BPNN. Further research on the comparison of fractional-order NNs to integer-order NNs are very necessary, such as fractional-order recurrent NN and convolutional NN. Moreover, the selection of fractional order, the influence of learning rate and other parameters on the FO BPNN are worthy of investigation.

REFERENCES

Chaoui, H. and Gualous, H. (2016). Adaptive state of charge estimation of lithium-ion batteries with parameter and thermal uncertainties. *IEEE Transactions on Control Systems Technology*, 25(2), 752–759.

Chin, C. and Gao, Z. (2018). State-of-charge estimation of battery pack under varying ambient temperature using an adaptive sequential extreme learning machine. *Energies*, 11(4), 711.

Densmore, A. and Hanif, M. (2016). Modeling the condition of lithium ion batteries using the extreme learning machine. In *2016 IEEE PES PowerAfrica*, 184–188. IEEE.

Guha, A. and Patra, A. (2018). Online estimation of the electrochemical impedance spectrum and remaining useful life of lithium-ion batteries. *IEEE Transactions on Instrumentation and Measurement*, 67(8), 1836–1849.

Hannan, M.A., Lipu, M.S.H., Hussain, A., Saad, M.H., and Ayob, A. (2018). Neural network approach for estimating state of charge of lithium-ion battery using backtracking search algorithm. *Ieee Access*, 6, 10069–10079.

Li, S., Hu, M., Li, Y., and Gong, C. (2019a). Fractional-order modeling and soc estimation of lithium-ion battery considering capacity loss. *International Journal of Energy Research*, 43(1), 417–429.

Li, Y., Liu, K., Foley, A.M., Zülke, A., Berecibar, M., Nanini-Maury, E., Van Mierlo, J., and Hoster, H.E. (2019b). Data-driven health estimation and lifetime prediction of lithium-ion batteries: A review. *Renewable and Sustainable Energy Reviews*, 113, 109254.

Mawonou, K.S., Eddahech, A., Dumur, D., Beauvois, D., and Godoy, E. (2019). Improved state of charge estimation for li-ion batteries using fractional order extended kalman filter. *Journal of Power Sources*, 435, 226710.

Nasser-Eddine, A., Huard, B., Gabano, J.D., and Poinot, T. (2019). A two steps method for electrochemical impedance modeling using fractional order system in time and frequency domains. *Control Engineering Practice*, 86, 96–104.

Pan, H., Lü, Z., Wang, H., Wei, H., and Chen, L. (2018). Novel battery state-of-health online estimation method using multiple health indicators and an extreme learning machine. *Energy*, 160, 466–477.

Rumelhart, D.E., Hinton, G.E., Williams, R.J., et al. (1988). Learning representations by back-propagating errors. *Cognitive modeling*, 5(3), 1.

Sheng, D., Wei, Y., Chen, Y., and Wang, Y. (2019). Convolutional neural networks with fractional order gradient method. *arXiv preprint arXiv:1905.05336*.

Tarasov, V.E. (2016). On chain rule for fractional derivatives. *Communications in Nonlinear Science and Numerical Simulation*, 30(1-3), 1–4.

Wei, Z., Xiong, B., Ji, D., and Tseng, K.J. (2017). Online state of charge and capacity dual estimation with a multi-timescale estimator for lithium-ion battery. *Energy Procedia*, 105, 2953–2958.

Yang, J., Peng, Z., Wang, H., Yuan, H., and Wu, L. (2018). The remaining useful life estimation of lithium-ion battery based on improved extreme learning machine algorithm. *Int. J. Electrochem. Sci*, 13, 4991–5004.

Zahid, T., Xu, K., and Li, W. (2017). Machine learning an alternate technique to estimate the state of charge of energy storage devices. *Electronics Letters*, 53(25), 1665–1666.

Zahid, T., Xu, K., Li, W., Li, C., and Li, H. (2018). State of charge estimation for electric vehicle power battery using advanced machine learning algorithm under diversified drive cycles. *Energy*, 162, 871–882.

Zhang, Q., Shang, Y., Li, Y., Cui, N., Duan, B., and Zhang, C. (2019). A novel fractional variable-order equivalent circuit model and parameter identification of electric vehicle li-ion batteries. *ISA Transactions*.

Zhu, Q. et al. (2018). A state of charge estimation approach based on fractional order adaptive extended kalman filter for lithium-ion batteries. In *IEEE 7th DDCLS*, 271–276.